THE ASTROPHYSICAL JOURNAL, 297:476–491, 1985 October 15

RADIATIVE SHOCK-WAVE THEORY. II. HIGH-VELOCITY SHOCKS AND THERMAL INSTABILITIES

LUC BINETTE,[1] MICHAEL A. DOPITA,[2] AND IAN R. TUOHY[2]
Received 1982 November 10; accepted 1985 April 18

ABSTRACT

The ionization structure and emission spectrum (optical and infrared) produced by low-density plasma cooling from initial temperatures as high as $10^{7.2}$ K are investigated. For initial temperatures higher than $10^{5.4}$ K, the optical spectra are dominated by emission from the low-temperature ($\sim 10^4$ K) photoionized regions that result from reabsorption of EUV ionizing flux emitted in the high-temperature zones. The predicted line intensities compare favorably with the emission filaments observed in M87 and NGC 1275, which are here assumed to result from cooling of an intracluster X-ray–emitting hot gas. A certain ambiguity makes it difficult in practice to choose between the latter models and pure photoionization models.

Subject headings: atomic processes — galaxies: nuclei — interstellar: matter

I. INTRODUCTION

Our understanding of the structure of radiative shocks of modest ($50 \lesssim V_s \lesssim 200$ km s^{-1}) velocity has improved greatly since the pioneering work of Cox (1972). This advance has been accomplished primarily by the use of more complex physics in the shock front and its precursor, and the cool recombination zone. The models of Dopita (1976, 1977), for example, followed the development of the ionization structure from the initial conditions down to the final recombination zone, instead of assuming that collisional ionization equilibrium is set up immediately in the postshock gas. The models of Raymond (1979) dealt with the problem of the structure of the recombination zone, allowing for the diffusion of ionizing photons produced in the hot gas into this zone. However, both these models and those of Dopita assumed arbitrary preionization. This assumption was raised by Shull and McKee (1979), who considered the effects of the diffusion of ionizing photons into the preshock gas. By treating the ionizing precursor as a simple one-zone R-type ionization front, they were able to produce self-consistent shock models. A rather different effect is that due to temperature relaxation between the heavy particles and the electrons in the postshock gas. This was shown to be important in low-velocity shocks for which hydrogen was not appreciably preionized. This occurs for $V_s \lesssim 80$ km s^{-1}.

The importance of charge transfer reactions was assessed by Butler and Raymond (1980). Shull (1980) and Draine (1981) have considered dust emission in the shock structure. In none of these models does the velocity exceed 200 km s^{-1}. In part, the reason for this is that the computational complexity becomes very great, since all stages of ionization and their cooling processes must be considered. However, the major reason has been that for $V_s > 200$ km s^{-1}, cooling time scales for the hot plasma become much longer than any other relevant time scale in supernova remnants (SNR) to which the models have been mainly applied. Such high-velocity shocks thus have no physical significance in these objects.

At very high density, ($N_e \gtrsim 10^6$ cm^{-3}), cooling time scales again become short, and high-velocity models become relevant to the physics of active galactic nuclei. Daltabuit and Cox (1972) suggested that the high-velocity collision of two gas clouds of high density might, in various ways, resemble a quasi-stellar object and that such events might be relatively common during the early stages of galaxy formation. This idea was developed in a later paper (Daltabuit, MacAlpine, and Cox 1978), which considered the detailed structure and spectrum produced by a collision of two clouds of density 10^7 cm^{-3} at a relative velocity of 2000 km s^{-1}. Such high high velocities mean that the principal means by which the plasma cools in the postshock region is by thermal bremsstrahlung and line emission. This generates a soft X-ray radiation field which can be reabsorbed either in the shock precursor or in the recombination zone. The structures computed by Daltabuit, MacAlpine, and Cox (1978) therefore are symmetrical about the contact discontinuity between the two clouds and contain (in order, working outward) inner photoionization transitions, inner cooling to photoionization transitions, cooling zones, shock fronts, and outer photoionization precursors. The photoionized regions of this structure contain large fluxes of X-ray photons, so Auger processes must be fully accounted for.

The detection of optical filaments associated with galactic jets, of which Cen A is the best example (Blanco *et al.* 1975; Osmer 1978; Graham and Price 1981), suggests the possibility that low-density, high-temperature gas can become radiative on galactic distance scales. A low-density, high-velocity radiative shock would be the appropriate model in this situation. Another class of objects to which such a model may apply are the filaments in NGC 1275 (Kent and Sargent 1979) and M87 (Ford and Butcher 1979). These are most likely the result of cooling in an intracluster X-ray–emitting reservoir of hot gas, the source of which is possibly pressure stripping of cluster members. Fabian and Nulsen (1977), Mathews (1978) and Mathews and Bregman (1978) find that, in the potential well of massive galaxies such as M87, the hot gas is likely to cool in a thermally unstable fashion (Field 1965). In this case, illumination of the cooling gas by the soft X-rays of the surrounding medium should produce a spectrum not unlike a high-velocity, low-density radiative shock wave. The models presented in this paper as well as those of Contini and Aldrovandi (1983) investigate what kind of emission can be expected from such a structure where shock velocities as high as 1080 km s^{-1} are

[1] European Southern Observatory, Garching bei München.
[2] Mount Stromlo and Siding Spring Observatories, Australian National University.

envisaged. Unlike the models of Contini and Aldrovandi, which further consider the effects of an external ionizing source of arbitrary intensity and spectral index, in this paper we limit ourselves to the self-consistent case where the important UV ionizing flux is produced only in the high-temperature zone of the shock flow. The intensity and detailed energy spectrum of the ionizing flux were derived from the Raymond and Smith (1977) code, which, in the case of very hot plasma, more accurately computes the emissivities in the ultraviolet. A fraction of this UV flux reaches the cooler recombination zone and will be shown to considerably alter its ionization structure. The flow quantities and the optical spectrum were calculated with the computer code MAPPINGS described in the Appendix.

II. THE MODELS

a) Steady-Flow Models

Since the computer code MAPPINGS which is described in the Appendix includes atomic data only on the first six ionization stages of heavy elements, it cannot, in conditions of collisional ionization equilibrium, describe a plasma with $T_e \gtrsim 2 \times 10^5$ K. However, except for a few coronal lines such as [Fe XIV] λ5303, it is the region of a shock below $T_e \approx 2 \times 10^5$ K which produces all the infrared, optical, and ultraviolet emission lines above the Lyman limit. Hotter zones produce hard UV and soft X-ray photons which are reabsorbed in the cooler part of the shock. It is these photons which alter the structure of the recombination zone and, by consequence, the optical spectrum.

We have therefore adopted the following modeling procedure. For the region above 2×10^5 K (hereafter the reference temperature T_r), we have assumed the plasma at any temperature to be optically thin and in conditions of collisional ionization equilibrium. The latter assumption is the most serious approximation of these models, since time scales for ionization of helium and hydrogen-like ions can be comparable to the bulk plasma cooling time scale, and the electron gas may be out of equipartition with the ions. Such effects have been considered in the case of the X-ray spectra emitted by adiabatic supernova remnant shocks (Itoh 1979; Gronenschild 1979; Gronenschild and Mewe 1982; Hamilton, Sarazin, and Chevalier 1983). A lower electron temperature results in low free-free continuum emission with a steeper slope toward high energies, and the lower ionization produced in nonequilibrium shocks enhances the line emissivity. With these caveats in mind, let us continue.

The output photon spectrum of the cooling plasma in the hot region will approximate to the sum of contributions of isobaric constant-temperature zones, weighted according to the change in heat capacity of the gas for the temperature interval considered, up to the initial temperature. The emissivity of the plasma in each of the 230 frequency bins in the energy range 7.64–5000 eV was computed using the Raymond-Smith code (Raymond and Smith 1977; Raymond, Cox, and Smith 1976). For an infinite slab, half of the radiation so emitted impinges on the surface of the zone at $T_r = 2 \times 10^5$ K. Examples of the photon source files so generated are shown in Figures 1*a*–1*c*; the hydrogen density at the reference temperature T_r is taken as 10 cm^{-3} (N_r). This ensures that collisional de-excitation effects are unimportant in the photoionized zone ($T_e \sim 10^4$ K), so that the models are appropriate in the low-density limit.

In the case of cooling plasma in a galactic jet or in the case of filaments with nonplanar geometries, such a photon field will overestimate the importance of the hotter plasma, since in a slab of finite cross section the hot zone will be sufficiently far from the recombination zone that only a fraction of the radiation emitted in the former is intercepted by the latter. In view of this problem, we adopt the following procedure: we first compute the Rankine-Hugoniot conditions assuming the initial temperature (hereafter T_i) to correspond to the postshock temperature, and with a preshock density such that the electron density, when the gas has cooled to T_r, is 10.0 cm^{-3} (N_r). The abundances[3] are solar (Allen 1973) and the magnetic field nil. On this basis, a cooling distance can be associated with each initial temperature, and this in turn determines the fraction of radiation emitted which reaches the recombination zone. The radius of the cooling cylinder of gas is assumed fixed, and the photon fields are computed for the set of radii 100 pc, 1 kpc, 10 kpc, and ∞.

It is found that the effect of limiting the radius of the cooling plasma was almost exactly the same as lowering the initial temperature. Compare, for example, Figures 1*d* and 1*b*, which show that the spectrum received in the recombination zone by a 100 pc radius cylinder cooling from $10^{7.0}$ K and an infinite slab cooling from $10^{6.6}$ K are to all intents and purposes identical. Because of this, only an infinite-slab set of models was computed.

Because the emissivity of a plasma of constant temperature declines approximately exponentially with photon energy, the output spectrum is a weighted sum of these exponentials. As Figure 1 shows, this can be approximated to a fair degree by a power law with a spectral index $\alpha \sim -0.5$ up to about 1 keV, with a much steeper slope at higher energies. We would therefore expect that, where the hard UV/soft X-ray field dominates the structure of the recombination zone, the emitted spectrum should be similar to that produced by a nonthermal source. Such an expectation is borne out by computation.

The emission-line spectrum was computed by inputting one of the integrated photon sources into a plane-parallel steady-flow shock model, with initial conditions given above. The ionization state at T_r of the heavy elements was that appropriate to the combined collisional ionization and photoionization equilibria at 2×10^5 K (including the photon source field). For $T_i < 10^6$ K, however, a relaxation time was computed, and the resulting ionization state is intermediate between equilibria and the preionization states derived from self-consistent models. Starting from T_r, the subsequent cooling, recombination, and absorption of the photon field were followed until the fractional ionization was less than 1%. This was typically reached after some 250 computation steps at temperatures of a few hundred degrees Kelvin. The models are characterized by 10 $\log_{10} T_i$ (example: model B60 has $T_i = 1.0 \times 10^6$ K), and Table 1 gives the spectra calculated for the full steady-flow models for a set of these temperatures from $10^{7.2}$ down to $10^{5.4}$ K. If these represented postshock temperatures, they correspond to shock velocities (with full preionization), of from 1080 km s^{-1} down to 130 km s^{-1}. Also given, for comparison purposes, in Table 1 is a fully self-consistent (cf. Shull and McKee 1979) shock model using the same abundances and a postshock temperature of $10^{5.2}$ K. This gave hydrogen and helium (He^+) preionizations of 0.41 and 0.39, respectively, and

[3] These abundances relative to hydrogen by a number are He:C:N:O:Ne:Mg:Si:S:Cl:Ar = (850:3.3:0.91:6.6:0.83:0.26:0.33:0.16:0.004:0.063) $\times 10^{-4}$.

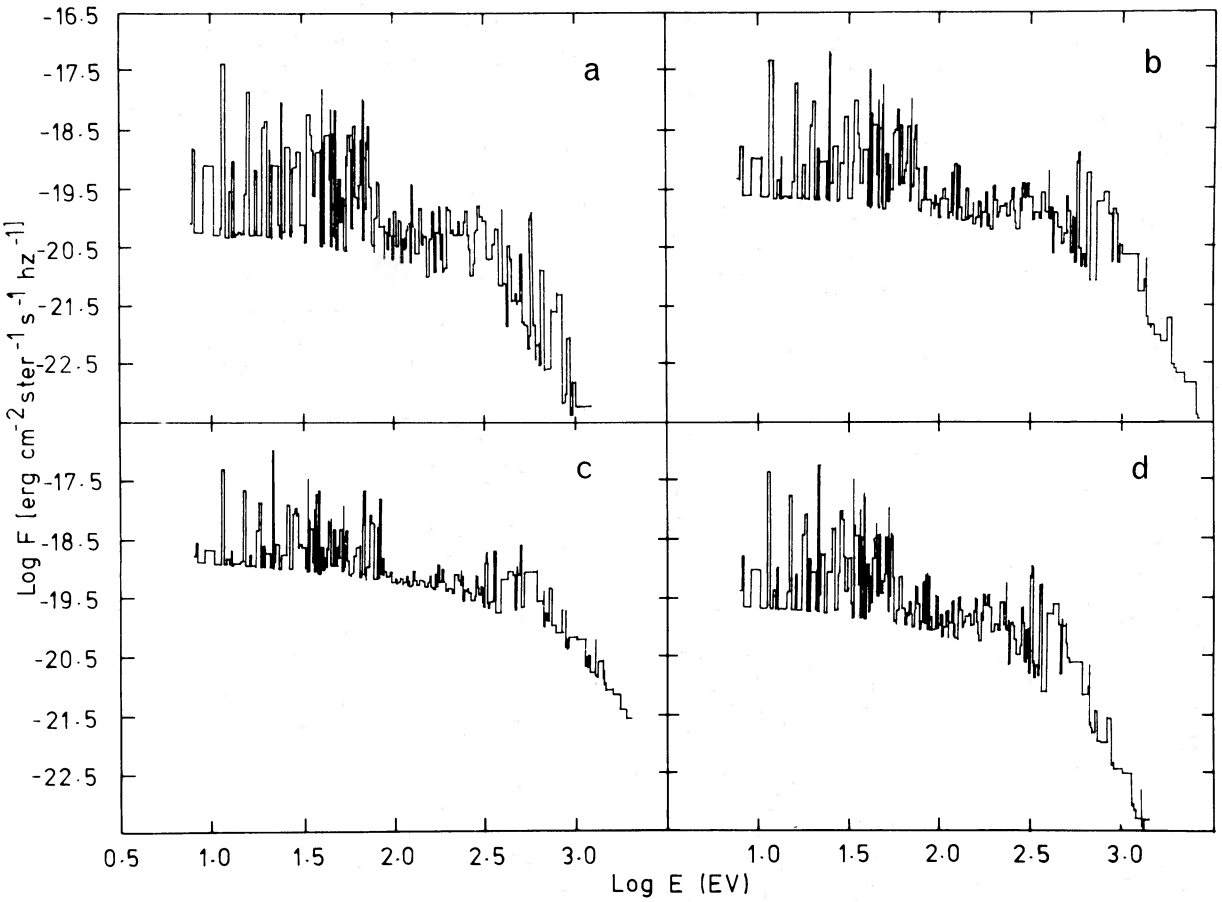

FIG. 1.—(*a–c*) Ionizing fluxes reaching the zone at $T_r = 2.0 \times 10^5$ K ($N_r = 10$ cm^{-3}) for initial temperatures T_i of (*a*) $10^{6.2}$, (*b*) $10^{6.6}$, and (*c*) $10^{7.2}$ K, respectively, in the case of infinite slabs. (*d*) T_i is $10^{7.0}$ K, and the emitting cylinder has a radius of 100 pc.

a shock velocity of 86 km s^{-1}. Apart from slight differences in the set of abundances and in the preionization, this corresponds roughly to Shull and McKee's model D. It can also be compared to the Cygnus Loop model[4] of Binette *et al.* (1982), which has comparable preionization values but for which the spectrum is more dissimilar because of the reduced abundances employed. It is apparent that for $T_i \gg 10^{5.3}$ K, the effect of the ionizing radiation becomes progressively more important. This generates a zone of photoionization equilibrium when the temperature is about 10^4 K which becomes thicker as T_i rises. The emission from this zone gradually dominates the observed spectrum, resulting in a weakening of the UV resonance and intercombination lines and a strengthening of the optical and IR forbidden lines with respect to Hβ.

This point is graphically illustrated by the computed ionization and temperature structures (Fig. 2). For the model shown, B60 ($\log_{10} T_i = 6.0$), the gas initially cools and recombines as if there were no ionizing radiation field. However, when the temperature reaches 8300 K, the heating effect of the radiation field dominates and the plasma readjusts to form an isobaric slab in photoionization equilbrium. This state of affairs continues until the ionizing field is exhausted, at which point the temperature collapses, leading to a rapid increase of density.

Table 2 shows for each model the computed shock velocity (T_i corresponding to the postshock temperature T_2), the absolute Hβ flux, and Q(H)/A, the flux number of ionizing photons reaching the zone at T_r. Because the number of ionizing photons rises steeply with T_i, the average number of recombinations which hydrogen undergoes in making its way from the shock front to the cold recombined region also increases steadily, and this is why the Hβ flux grows almost linearly with T_i. We also give the distances required for the gas to cool from T_i to T_r (isobarically) (d_r), from T_r to 11,000 K ($d_{11,000}$), and from 11,000 K to 1000 K (d_{1000}). This shows how rapidly the effect of photoionization makes itself felt. Note that for $T_i \gtrsim 10^{6.2}$ K, photoionization effects are becoming important even in the hotter plasma. Table 2 includes some electronic temperatures and densities averaged over the emissivity of a few interesting ions. On the whole, average temperatures decrease markedly with Q(H) owing to the increasing weight of the isothermal zone. In the case of [N II], however, the ionic temperature variations are not so large.

The time scale over which the flow must persist and ensure the buildup of a steady-flow situation *and* full absorption of the radiation field increases as the initial temperature is raised. For $T_i > 10^{6.2}$ K, t_{abs} nevertheless becomes shorter than the cooling time scale for the hot plasma, t_{cool}. This is illustrated by Figure 3, which shows the two time scales as a function of

[4] The shock velocity (120 km s^{-1}) in the latter model is somewhat too high for the low preionization values obtained, and results from the incompleteness of the mechanisms responsible for preionization that were included in the first version of MAPPINGS.

TABLE 1

EMISSION-LINE SPECTRA GIVEN BY MODELS:[a] OPTICAL AND INFRARED LINES

λ(Å)	3721	3725	3728	3869	3889	4068	4076	4102	4340	4363	4471	4686
ION	[SIII]	[OII]	[OII]	[NeIII]	HeI	[SII]	[SII]	Hδ	Hγ	[OIII]	HeI	HeII
B52	0.8	662	918	6.1	6.6	22.6	7.4	24.3	45.1	7.3	3.0	0.67
B53	1.5	502	641	51.6	9.6	22.0	7.1	25.0	45.9	36.4	4.4	25.7
B54	0.7	258	329	24.1	4.9	13.4	4.3	25.1	45.8	16.3	2.3	11.8
B58	0.5	234	297	10.9	11.4	21.5	7.0	25.5	46.3	7.2	5.5	6.6
B60	0.8	291	364	9.3	14.3	26.3	8.6	25.6	46.4	4.1	6.8	7.0
B66	2.0	503	627	23.7	13.8	26.4	8.6	25.7	46.6	1.2	6.4	10.8
B72	3.9	608	781	49.0	14.5	37.1	12.1	25.5	46.3	0.58	6.6	16.6
D58	0.3	137	172	11.9	11.3	8.6	2.8	25.0	45.8	7.9	4.9	4.9

λ(Å)	4861	4959	5007	5199	5517	5577	5755	5876	6300	6310	6363	6548
ION	Hβ	[OIII]	[OIII]	[NI]	[ClIII]	[OI]	[NII]	HeI	[OI]	[SIII]	[OI]	[NII]
B52	100	35.4	102	26.8	1.3	0.4	8.3	9.0	43.5	1.3	13.5	65.2
B53	100	186	536	21.4	1.4	0.5	8.3	13.1	70.0	2.6	21.7	86.4
B54	100	82.4	238	18.3	0.6	0.3	4.1	6.7	65.6	1.2	20.4	52.1
B58	100	32.9	95.0	60.9	0.5	0.8	2.9	16.1	222	0.9	69.1	78.9
B60	100	18.5	53.4	83.7	0.9	1.7	3.7	19.5	326	1.4	101	116
B66	100	10.5	30.4	109	1.9	2.9	6.5	17.9	435	3.4	135	165
B72	100	16.7	48.2	284	2.5	73	8.7	18.5	937	6.7	291	175
D58	100	38.0	110	12.3	0.3	0.1	1.9	15.5	59.0	0.6	18.3	49.1

λ(Å)	6563	6583	6717	6731	7136	7317	7328	7751	8577	9069	9123	9526
ION	Hα	[NII]	[SII]	[SII]	[ArIII]	[OII]	[OII]	[ArIII]	[ClII]	[SIII]	[ClII]	[SIII]
B52	300	192	222	176	16.7	43.3	34.8	4.0	1.5	4.9	0.4	11.9
B53	304	254	205	176	20.5	26.2	21.0	4.9	1.9	17.3	0.5	42.2
B54	304	153	176	153	9.8	12.7	10.2	2.3	2.1	8.2	0.6	19.9
B58	295	232	374	308	12.1	7.9	6.4	2.9	4.9	14.7	1.3	35.8
B60	292	342	418	338	25.5	6.9	5.5	6.1	5.5	28.9	1.5	70.4
B66	290	487	402	313	44.3	11.4	9.1	10.6	5.8	59.0	1.6	144
B72	297	515	641	475	59.5	16.0	12.7	14.2	10.9	105	3.0	255
D58	307	145	158	143	6.6	6.0	4.8	1.6	2.4	8.3	0.7	20.2

λ(μ)	1.03	4.49	8.00	8.99	12.79	15.55	18.92	33.65	34.81	63.07	121.0	156.0
ION	[SII]	[MgIV]	[ArII]	[ArIII]	[NeII]	[NeIII]	[SIII]	[SIII]	[SiII]	[OI]	[NII]	[CII]
B52	20.1	-	25.5	8.4	125	1.4	3.6	5.3	655	26.6	6.8	46.9
B53	19.5	0.6	31.7	14.6	165	11.0	17.9	25.5	682	37.3	7.5	37.1
B54	11.9	0.4	48.0	7.2	172	5.3	9.0	12.9	828	47.8	7.6	49.4
B58	19.1	2.0	70.8	16.1	316	4.9	26.1	40.1	1070	77.8	14.1	95.2
B60	23.4	3.0	62.9	30.0	345	12.2	44.7	68.0	989	80.3	18.0	99.6
B66	23.4	16.4	55.7	40.3	337	35.3	77.4	117	782	86.9	19.8	128
B72	32.9	88.4	121	50.9	642	53.2	135	209	1540	194	20.2	347
D58	7.6	2.3	91.1	16.2	390	6.4	27.7	42.6	1500	75.6	16.5	85.7

[a] Fluxes are relative to Hβ: $L(\mathrm{H}\beta) = 100.0$.

initial temperature. These scale inversely with the density. Were the age of the shock shorter or of the same order as these time scales, the flow structure would be similar to that encountered for the optically thin case, which is discussed in the next section. The cooling time scale is defined as

$$t_{\rm cool} = \int_{11,000}^{T_i} \frac{5k}{\epsilon(T)N(T)}\,dT = \int_{11,000}^{T_i} \frac{5kT}{\epsilon(T)N_r T_r}\,dT\ ,$$

where k is the Boltzmann constant, T_i is the initial temperature, and $\epsilon(T)$ is the emissivity of the plasma given by the Raymond-Smith code. (Raymond and Smith 1977; Raymond, Cox, and Smith 1976). The time scale for absorption of the UV radiation field is here defined as the time scale of passage of an atom through the zone of the model where the heating rate due to the radiation field exceeds half the cooling rate by atomic processes. Because heating becomes comparable to cooling processes only when the plasma has cooled to $T_e \approx 11{,}000$, $t_{\rm abs}$ is nearly identical with the cooling time from 11,000 K (to about 1000 K, the size of this absorption region being given by d_{1000} in Table 2).

b) *Finite Age/Optically Thin Models*

The physical reality of the plane-parallel steady-flow models becomes questionable at the higher velocities. This is because the gas in the cooling zone is usually thermally unstable (Field 1965) and will collapse into sheets or filaments if a small initial density perturbation is present (McCray, Stein, and Kafatos 1975; Chevalier and Theys 1975; Mufson 1975). In low density and in the presence of conduction, the condition for thermal stability is simply (Schwartz, McCray, and Stein 1972)

$$d\epsilon(T)/d\,\log\,T > 2\ .$$

However, the cooling rate given by the Raymond-Smith code can be approximated by

$$\epsilon(T) = 1.6 \times 10^{-19} T^{-1/2}\ \mathrm{ergs\ cm^3\ s^{-1}}$$

in the range $10^5 \lesssim T \lesssim 10^8$ K. Hence almost the whole cooling zone is thermally unstable to the condensation mode. For either high-velocity shocks or thermal instabilities developing out of a hot pool of gas, the characteristic scale length of the instability (i.e., the fastest growing mode) will determine the

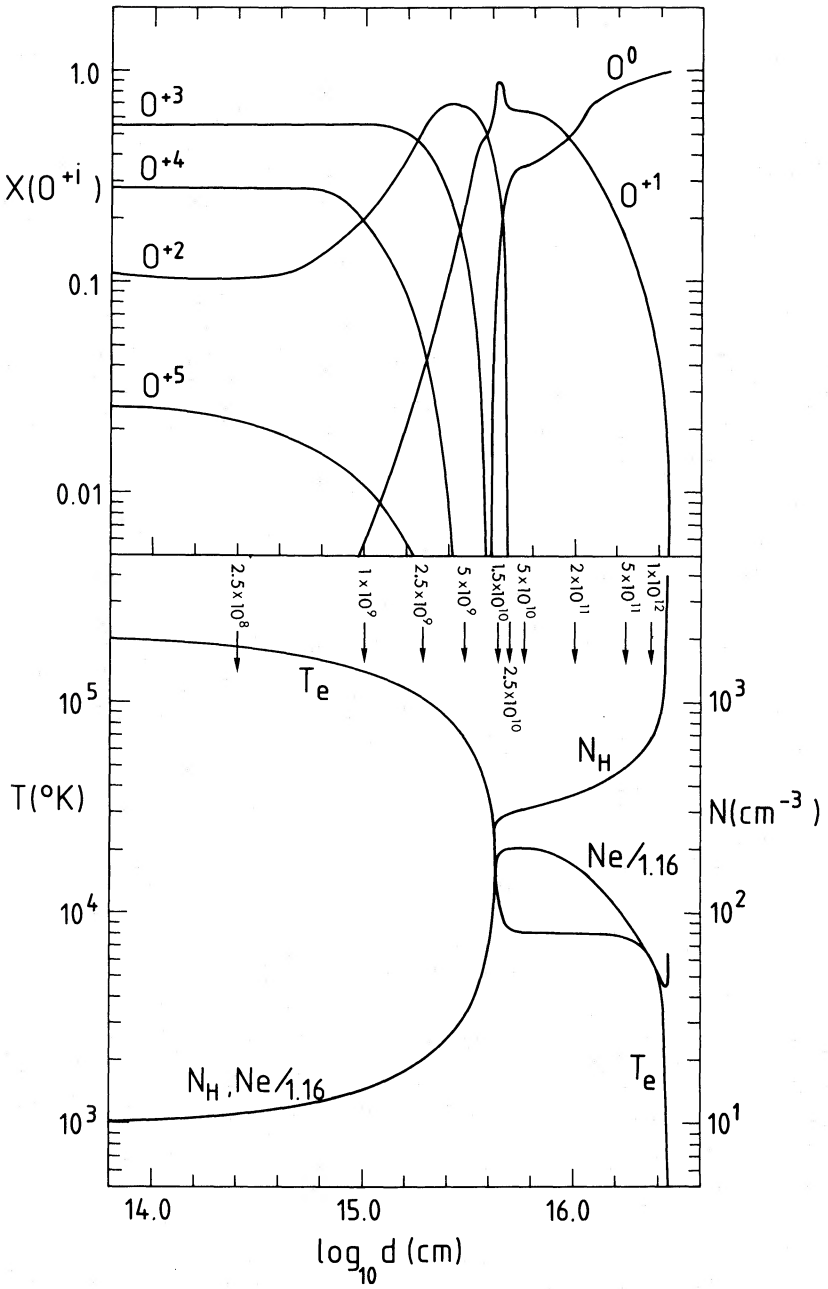

FIG. 2.—*Lower panel:* Flow variables for the model B60: hydrogen total density N_H, electron density N_e (divided by 1.16), and electron temperature T_e, as a function of distance from the zone at $T_r = 2.0 \times 10^5$ K. For the positions given by the arrows, the cooling times from T_r are indicated (s). *Upper panel:* Diagram gives the fractional ionization of oxygen as a function of distance.

column density of gas in these sheets or filaments, and this will be much smaller than in the models above which represent cooling of the plasma in bulk.

In order to check what effect this has on the output spectrum, equilibrium isobaric radiation-bounded plane-parallel photoionization models were constructed in which cloudlets were placed in the radiation field with a volume filling factor initially equal to the ratio of the initial photoionized equilibrium temperature and the initial temperature of the hot plasma. If all the input radiation field is absorbed, the spectra of the shock and photoionized models were quite similar as far as low-ionization species were considered (e.g., O I, O II, N I, N II, S II, S III, ...). This result arises because the specific intensity of the radiation field is similar in the two cases. The higher ionization lines were, however, markedly reduced in the photoionized models because of the absence of any region corresponding to the higher temperature cooling zone of shocks (2.0×10^5–2.0×10^4 K).

In the case of partially developed thermal instabilities, a density-limited (rather than ionization-limited) photoionized model will generally be more appropriate, because the clouds will not have completely absorbed the hard UV/soft X-ray radiation. This situation would be roughly equivalent to a shock of finite age. When the radiation field is not fully

TABLE 2

QUANTITIES CHARACTERIZING THE WAKE OF SHOCK MODELS[a, b]

MODEL	V_s (km.s^{-1})	$\log_{10}$ L(Hβ)/A[c] (erg.s^{-1}.cm^{-2})	Q(H)/A[c,d] (cm^{-2}.s^{-1}.10^8)	$\log_{10}$ d_r(cm)	d_{11000} (cm.10^{16})	d_{1000} (cm.10^{16})	$\langle T_e \rangle_{OIII}$ (°K)	$\langle N_e \rangle_{OIII}$ (cm^{-3})	$\langle T_e \rangle_{OII}$ (°K)	$\langle T_e \rangle_{NII}$ (°K)	$\langle N_e \rangle_{SII}$ (cm^{-3})	$\langle T_e \rangle_{SII}$ (°K)
B52	86	-4.97	-	-	0.55	0.71	31200	44	28400	8100	170	14600
B53	116	-4.88	-	-	0.35	0.44	26900	92	21800	8400	270	14400
B54	131	-4.62	0.03	14.76	0.32	0.53	27000	86	20900	7200	250	10500
B56	167	-4.63	0.19	16.37	0.30	0.69	27800	77	20000	7000	220	8700
B58	212	-4.46	0.48	17.26	0.37	1.38	28300	71	16000	7400	210	7800
B60	268	-4.23	1.01	18.01	0.43	2.73	21800	71	11500	8000	200	8000
B62	341	-4.04	1.55	18.83	0.97	4.80	16500	78	10300	8600	140	8400
B64	427	-3.84	2.30	19.61	0.78	6.37	12000	117	9500	8800	130	8400
B66	541	-3.77	3.08	20.32	0.62	11.3	11200	146	9600	9200	110	8300
B68	679	-3.69	3.79	20.97	0.50	21.6	10800	164	9800	9500	90	8200
B70	856	-3.57	4.84	21.62	0.43	38.7	10800	177	10000	9800	80	8100
B72	1080	-3.37	6.70	22.31	0.40	67.0	10800	186	10300	10000	70	8000

[a] For other values of the couple (T_r, N_r): $L' = kL$, $Q' = kQ$, $d'_x = d_x/k$ with $k = (T'/T_r)[N(T')/N_r]$. The references values are $N_r = 10$ cm^{-3}, $T_r = 2.0 \times 10^5$ K.

[b] The *average* electronic densities and temperatures determined for the ions O III, O II, N II, and S II were weighted according to their respective line emissivities.

[c] The denominator A represents the shock transversal area (cm^2).

[d] Q(H) is the number of ionizing photons emitted in the high-temperature zone which reach the reference layer at 2.0×10^5 K.

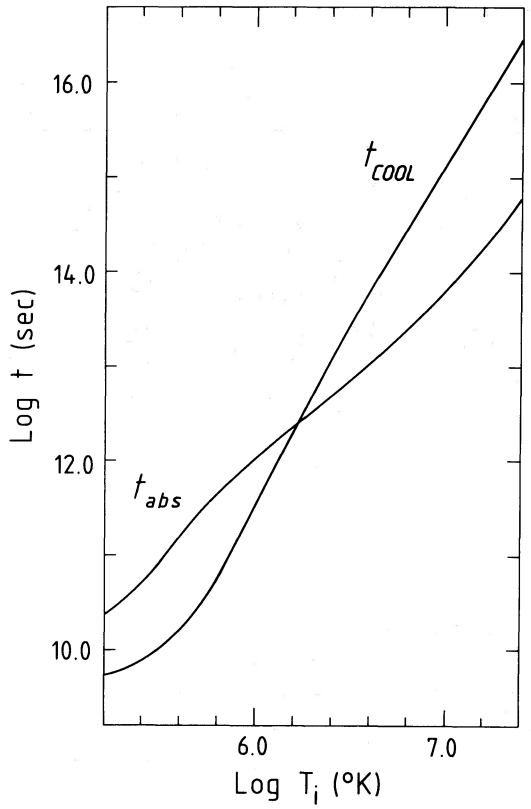

FIG. 3.—Cooling and absorption time scales as a function of initial temperature.

absorbed, the effect on the spectrum is to increase the relative strengths with respect to hydrogen of lines from high-excitation species at the expense of lines from neutral and singly ionized species. This is illustrated by the time tracks of the models in Figure 4, which is an excitation diagram used by Baldwin, Phillips, and Terlevich (1981) to distinguish among various excitation mechanisms. In this plot of $\log_{10}(\lambda 5007/\lambda 4861)$ against $\log_{10}(\lambda 3727/\lambda 5007)$, shock-excited objects are generally thought to lie in a region extending downward and to the right at roughly 45° from a point about $\log_{10}(\lambda 5007/\lambda 4861) = 0.5$, $\log_{10}(\lambda 3727/\lambda 5007) \approx 0.2$. This happens to correspond to the position occupied by our steady-flow models, as shown by the full line in Figure 4. Finite-age models, on the other hand, are found to populate a region that extends above and slightly to the right of the point mentioned. We must emphasize, however, that, in the low-density limit, these do not overlap the region occupied by power-law photoionized regions which is situated roughly at $\log_{10}(\lambda 5007/\lambda 4861) \sim 1.0$, $\log_{10}(\lambda 3727/\lambda 5007) \sim -0.4$ (cf. Baldwin, Phillips, and Terlevich 1981). On the other hand, as the density is increased, collisional de-excitation reduces the intensity of the [O II] $\lambda 3727$ lines. The segmented arrow in Figure 4, computed for $T_i = 10^{6.6}$, illustrates this point by showing the differential displacement of models' positions in the diagram with increasing density N_r. Densities of order 10^4 cm^{-3} in the zone at $T_e \approx 10^4$ K (i.e., $\sim 100 N_r$) or higher are required in order for the time tracks to overlap the above-mentioned region. The model described here is therefore ruled out for objects such as Cygnus A whose [S II] $\lambda 6717/\lambda 6731$ line ratio of 1.1 (Osterbrock and Miller 1975) implies an electron density as low as 3×10^2 cm^{-3} (at $T_e \approx 10^4$ K).

We must point out that in Figure 4 the early turnover of the ratio O II/O III with increasing temperature T_i, in the case of steady-flow B-series models with $T_i > 10^{5.3}$ K, is actually the result of a high rate for the charge transfer reaction: $O^{+2} + H^0 \rightarrow O^+ + H^+$. The rate coefficient used in the B-series models—7.8×10^{-10} cm s^{-1} ($T_e = 10^4$ K)—corresponds to the value of Butler, Heil, and Dalgarno (1980), which they derived from quantal calculations. Although models that completely neglect this reaction occupy quite a different position in the diagram, small variations in the coefficient rate are found to produce only moderate displacements of the B-series models; this is illustrated for model B66 by the broken-line arrow, which corresponds to a reduction of the coefficient by a factor 2. Because of the growing body of evidence, both observational (Péquignot, Stasińska, and Aldrovandi 1978; Péquignot 1980) and theoretical (Butler and Dalgarno 1980; Butler, Heil, and Dalgarno 1980), favoring a high rate for this reaction, significant changes in the locus of models are not expected. It is interesting to note that even though O III is a major coolant, the emission-line intensities from other atomic species (Table 1) have been found to be quite insensitive to the coefficient value for this reaction.

III. DISCUSSION

The models just described appear particularly well suited to the low-excitation emission filaments observed in M87 (Ford and Butcher 1979) and NGC 1275 (Kent and Sargent 1979), for which shock models have already been proposed. In the particular case of NGC 1275, it is the low-velocity system (labeled LV by Kent and Sargent) which is considered most likely to be shock-excited; the observed line widths (FWHM) in the LV system are quite large (350 km s^{-1}), while for the high-velocity system (HV) the lines are narrow and the gas excitation is significantly higher. Fabian and Nulsen (1977) interpreted the LV filaments as being condensations in the intracluster medium infalling toward the core of NGC 1275. Both of the galaxies that have been cited here as examples are situated deep in the gravitational well of X-ray–emitting clusters, a propitious environment for gas infall and condensation into filaments, as shown by the recent work of Stewart *et al.* (1984) on the importance of cooling flows in clusters of galaxies. In Figure 4 the agreement between the filaments' spectra and the locus of models is certainly encouraging, but caution must be exercised in interpreting the spectral data, since there remain sizable uncertainties in the measured line ratios due to factors such as reddening or underlying stellar absorption lines. For instance, in M87 the observed value for the Balmer decrement is 4.0, significantly in excess of the value of 3.00 ± 0.08 given by the models, and could result from the fact that the spectra have not been corrected for absorption. For Liners (low-ionization nuclear emission-line regions; cf. Heckman 1980) in general, where emission lines are weak compared with the stellar background of the parent galaxy, this type of correction has been shown not to be negligible (Stauffer 1982; Keel 1983*b*). Since Ford and Butcher (1979) have made a case for not attributing the large Balmer decrement in M87 to reddening, we have indicated by the dotted arrow in Figures 4–6 the effect of correcting (Balmer lines) for underlying absorption lines in order to reproduce the theoretical Balmer decrement. The supposedly corrected intensities would then favor model D58, whose only difference from B58 is that the abundances of heavy elements are doubled. It is interesting to note here that X-ray spectroscopy of the M87 hot gas also seems to suggest

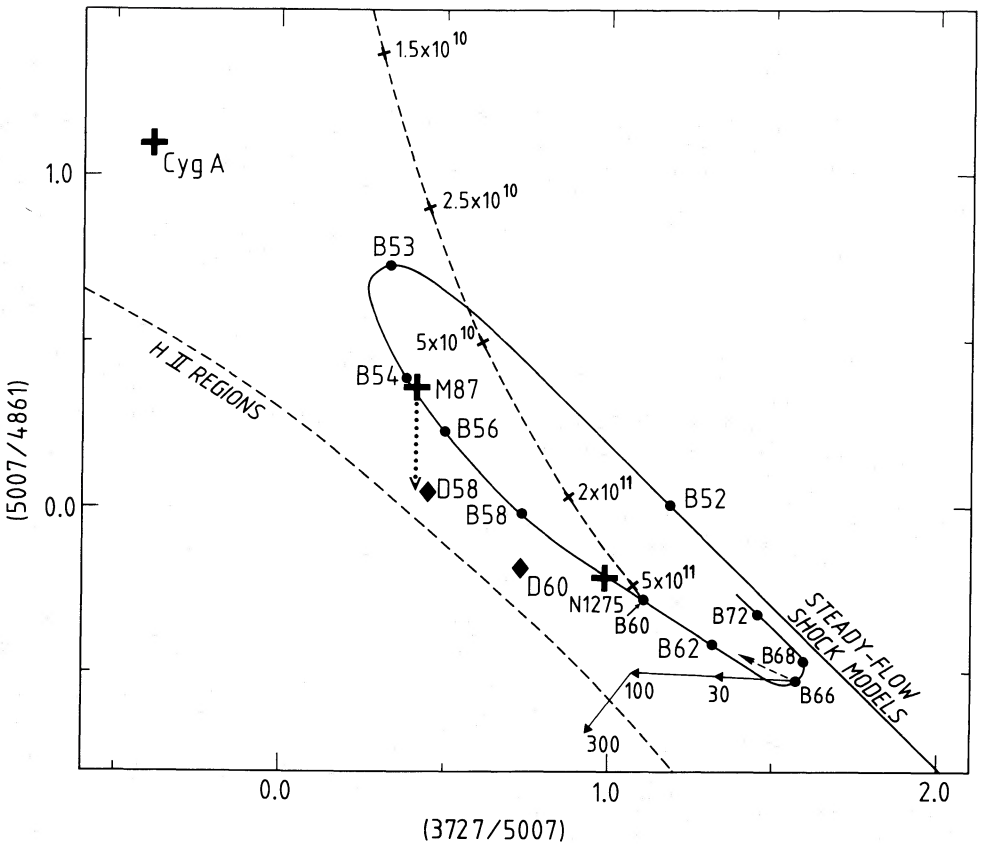

FIG. 4.—The [O III]/Hβ ratio as a function of the [O II]/[O III] ratio. The full line joins steady-flow shock models of the B series. The models D58 and D60 (*diamonds*) were computed using heavy-element abundances which were double the solar values (Allen 1973). The tick marks on the time track of model B60 (*broken line*) indicate the time elapsed (s) since $T_e = T_r$. The typical position of H II regions is given by the bottom broken line. The positions occupied by the emission spectra of Cygnus A and of the filaments in M87 and NGC 1275 (low-velocity filaments) are shown as crosses. The dotted arrow at the position of M87 gives an upper limit to the magnitude of the correction for the presence of underlying Hβ absorption line. For model B66, the segmented arrow shows the differential shift in the diagram if the density N_r is multiplied by factors of 30, 100, and 300, respectively, while the broken arrow indicates the effect of cutting in half the O^{+2} recombination charge transfer coefficient.

an overabundance of heavy elements, particularly oxygen, which has an abundance greater than about 1.5 times the solar value (Canizares *et al.* 1982). As for NGC 1275, the even larger Balmer decrement observed (of value 4.8) is, on the other hand, considered by Kent and Sargent (1979) to be entirely due to reddening, although, here also, effects of the absorption lines were not considered; the dereddened line ratios are plotted in Figures 4–6 corrected for $E(B - V) = 0.43$. For this object, model B60 appears to be the most satisfactory in Figure 4.

In Figure 5, which is another diagram of Baldwin, Phillips, and Terlevich (1982) where $\log_{10}$ (5007/4861) is plotted against $\log_{10}$ (6583/6563), the two objects and the models occupy a position quite distinct from H II regions but similar to Liners (cf. Fig. 8 in Stauffer 1982). If model B60 remains acceptable for NGC 1275, M87 is much to the right of the locus of steady state models. The abundance of nitrogen can be changed independently (without affecting line fluxes of other atomic species, since nitrogen plays a minor role in the cooling function) to fit the observations, but the required increase is quite large: 4.5–7.5 times the solar N/O ($\sim$0.14) abundance ratio depending on whether or not one applies the absorption correction. Although this is not unreasonable in the event of an enriched interstellar medium, as suggested by the relative success of D58 in Figure 4 (and Fig. 6), it is nevertheless a factor of 2 higher than the N/O ratio (=0.30) favored by photoionization models which were found to reproduce rather well the observed N II/O III line ratio in Liners (Binette 1985).

Among the few other optical lines observed in these objects are [O I] and [S II], which are plotted relative to Hα in Figure 6. (In the case of the [S II] doublet, it is preferable to plot only the [S II] λ6731 line, since it is less sensitive to de-excitation than [S II] λ6717.) The diagram indicates a significant reduction in the [O I] flux when abundances are increased; this results from the more rapid drop of the electronic temperature, in the partially ionized recombination zone, with increasing abundances. In Figure 6, it is only for the M87 absorption-corrected measurement that models remain acceptable, with model D58 again providing the best fit (other line intensities of D58 can be found in Table 1). In the case of NGC 1275, significant discrepancies between the measured intensities and the models remain.

It must be emphasized that the observed spectra still put too few constraints on models to enable firm conclusions about photoionization or shock excitation of the filaments in these particular objects to be drawn. Photoionization appears more successful in reproducing the whole range of excitation observed in nuclear emission galaxies. For instance, in a diagram (Binette 1984, 1985) of [O III]/(Hα/3) versus [O I]/[O III], three-quarters of galaxies with nuclear emission (but not H II region–like) discovered in the course of magnitude-

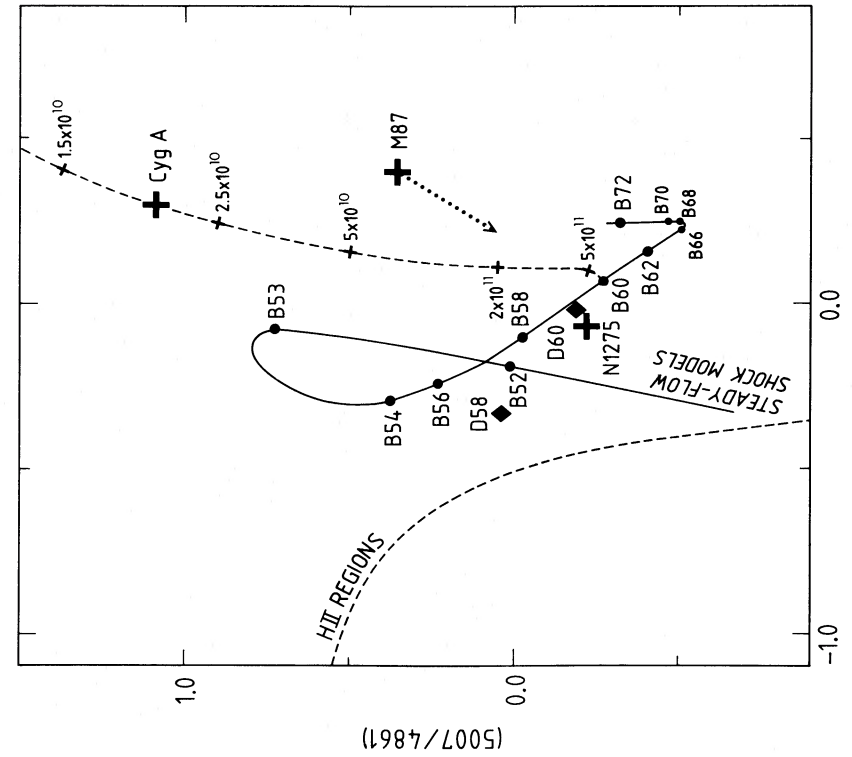

FIG. 5

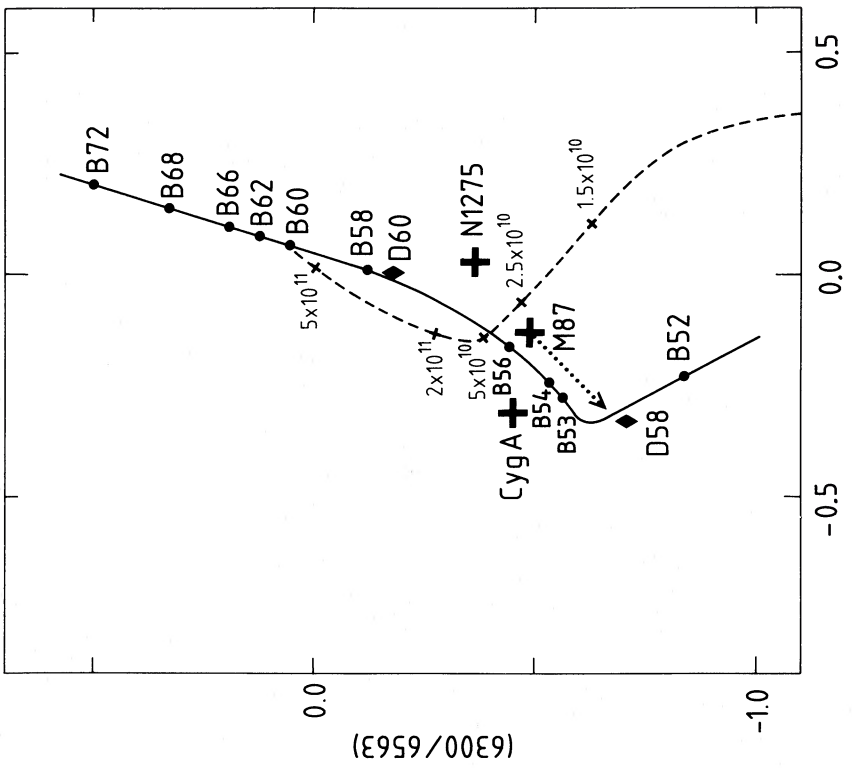

FIG. 6

FIG. 5.—[O III]/Hβ ratio as a function of the [N II]/Hα ratio. Symbols have the same meaning as in Fig. 4.
FIG. 6.—[O I]/Hα ratio as a function of the [S II]/Hα ratio. Symbols have the same meaning as in Fig. 4.

limited surveys fall inside a linear band which is only 0.3 dex wide (the span in [O I]/[O III] is 1.7 dex). A correlation between [N II]/[O III] and [O I]/[O III] also exists. The shock models given in Table 1 do not reproduce these correlations well (except when many parameters are varied simultaneously), while in the case of photoionization, they are successfully reproduced by varying the ionization parameter (cf. Binette 1985 and references therein). In any event, shock models overlap part of the sequences where typical Liners are found (at the position occupied by M87 in the diagrams), and, therefore, a basic ambiguity remains between the two types of models, at least for a fraction of Liners. Shock excitation as the dominant mechanism for some objects, as suggested by Stauffer (1982), cannot be ruled out. If this is the case, one should look at differences in the morphology or in the physical environment of the parent galaxy which would correlate with (and possibly justify) a different excitation mechanism. In this respect, M87 and NGC 1275 might give us a hint, since each has a preeminent position in its respective cluster. Furthermore, their optical emission (or part of it) has been spatially resolved into thick filamentary structures which are probably the result of infall from the intracluster medium. By contrast, a substantial fraction of Liners consists of isolated galaxies, many having a more or less uniform emission structure, others presenting a knotty or ringlike configuration (Keel 1983*a*; Demoulin-Ulrich, Butcher, and Bokenberg 1984). Increased spatial resolution of the emission could still, however, reveal finer filamentary structures as seen in NGC 7217 (see Fig. 12 of Keel 1983*a*). Even if both types of excitation mechanism were to operate to different degrees in different objects, one should note that the relative success of these new shock models (in Table 1 or Contini and Aldrovandi 1983) in reproducing the Liners' spectral signature is due to the superposing of a sufficiently large UV flux on the cooler downstream shock zone, which results in an extended quasi-equilibrium photoionized region. These particular shock models therefore represent a second-order effect compared with pure photoionization. Shocks, however, by means of a relatively flat UV ionizing spectrum (cf. Fig. 1) tend to reproduce the emission spectrum of photoionization with a steeper UV spectrum.

We are indebted to Dr T. Barnes for providing access to the University of Texas CYBER system on which the B-series models were computed.

APPENDIX

THE MODELING CODE

This paper is one in a series utilizing a new modeling code (MAPPINGS) developed by two of us (LB and MD). The latter is intended for use in modeling not only shocks (cf. Dopita *et al.* 1984; Dopita, Binette, and Tuohy 1984), but also H II regions and galactic nuclei, both in the steady and the time-dependent ionization cases. The complete description is by Binette (1982), but for reference in future papers we develop here the major features of the code.

I. DETERMINATION OF THE THERMAL BALANCE AND SPECTRUM

A major cooling mechanism is the collisional excitation of forbidden lines. It is computed by treating the atom or ion as a five-level system. The statistical equilibrium of the metastable states is calculated using the parameters listed is Osterbrock (1974) and the references therein, supplemented by recent data from Eissner and Seaton (1974), Seaton (1975), Dopita, Mason, and Robb (1976), Pradhan (1976, 1978), Bhatia, Doschek, and Feldman (1979), Nussbaumer and Rusca (1979), Zeippen (1982), and Mendoza and Zeippen (1982). Variations of collision strengths with temperature are included for O I and N I. The intensities (10 lines per ion) are computed for each of the following ions: O I, O II, O III, N I, N II, S II, S III, Ne III, Ne IV, Ne V, Ar III, Ar IV, Ar V, Cl II, Cl III and Cl IV. The atomic data are now being updated to include the recent compilation of Mendoza (1983) and to take into account dielectronic recombination at low electronic temperatures according to the prescription of Nussbaumer and Storey (1983).

Cooling resulting from the emission of 56 resonance lines is also computed. The temperature-averaged Gaunt factor used to derive the collision strength from the oscillator strength is obtained from Tarter (1969).[5] Collisional de-excitation for these lines is neglected. Finally, the cooling due to 47 intercombination or semiforbidden lines is computed. For these and the resonance lines we derived the collision strength using the compilation of oscillator strengths by Smith and Wiese (1971) and by Wiese, Smith, and Glennon (1966). In our computations we allow for collisional de-excitation of the upper level.

The intensities of the Balmer lines of hydrogen are computed up to Hϵ. The fraction of the emission due to recombination is calculated using the effective recombination coefficients of Brocklehurst (1971), which are dependent on both density and temperature. No cooling of the gas results from the emission of the lines themselves, since the (potential) energy released escapes the system. The fraction of the emission occurring through collisional excitation of neutral hydrogen, however, is often a major cooling agent at high temperature. It is calculated by determining the collisional excitation rates to the seven lowest leves of hydrogen, using the rates of Johnson (1972) as a function of temperature but adjusted to take into account the experimentally measured resonance structure reported by Kleinpoppen and Kraiss (1967) above threshold (cf. Dopita, Binette, and Schwartz 1982).

Baker and Menzel's (1938) case B is assumed for the recombination component of the Balmer lines throughout. However, for the collisionally excited component, neither case A nor case B is explicitly assumed, since collisional excitation can be important at the high-temperature end of shocks where velocity gradients are high, and, in consequence, optical depths in Lyman lines may be quite small. In this case, a linear combination of case A and case B based on the local optical depth in Lyγ is used, treating this as a resonance line by the Capriotti (1965) escape probability formulation (cf. § IV of this appendix).

[5] None of the oscillator strengths themselves were taken from Tarter.

The energy loss through recombination is computed using the coefficients $\beta_A(H^0, T)$ in Osterbrock (1974). The method was, however, generalized to other atomic elements, which were treated as hydrogen-like. With normal cosmic abundances, these loss rates are completely negligible in the case of heavy elements; however, their inclusion is necessary when there is an overabundance of these (as found in supernova ejecta, for example), and the code is intended to remain as realistic aad consistent as possible when such conditions are encountered. An illustration of the type of problem that one can hope to tackle is given by Dopita, Binette, and Tuohy (1984).

Helium (He^0) is treated as a five-level system. The collisional excitation rates to the $2\,^1S$, $2\,^1P$, or $2\,^3P$ levels from the $2\,^3S$ level are taken from Osterbrock (1974). The triplet states are assumed to be populated only by recombination, whereas for the singlets, collisional excitation from the ground state $1\,^1S$ is taken into account as well. The hydrogen-ionizing transitions $2\,^1P \rightarrow 1\,^1S$ (584 Å) and $2\,^3S \rightarrow 1\,^1S$ (591 Å), and the helium two-photon conuum $2\,^1S \rightarrow 1\,^1S$, are included in the ionizing radiation field.

The Lyman photons produced through recombination of He^{+2} and those (with the associated cooling) resulting from collisional excitation of He^+ are computed. The collisional excitation rates are from Johnson (1972).

The cooling rate due to collisional ionization is simply the multiplication of the collisional ionization rate (obtained from Cantó and Daltabuit 1974 and Franco and Daltabuit 1978 by the ionization potential of the ionic species considered.

Finally, the cooling due to free-free emission was calculated using the formula in Allen (1973) with the averaged Gaunt factor from Spitzer (1978).

The total heating rate G_T resulting from photoionization includes the contribution from each atomic species (X_j^{+i}), since, as was shown by MacAlpine (1972), the contribution to heating of elements heavier than H and He is significant when the UV source spectrum is flat and extends into the X-ray energies.

$$G_T = \sum_{j,\,i} G(X_j^{+i}) , \qquad 0 \leq i \leq 4 ,$$

where X_j^{+i} corresponds to the ionization stage i of atomic element X_j. The individual contributions to heating can then be written

$$G(X_j^{+i}) = N(X_j^{+i}) \int_0^{\infty} \frac{4\pi J_\nu}{h\nu} \sum_k a_{\nu k}(X_j^{+i})[h\nu - h\nu_{0k}(X_j^{+i}) + h\nu_{Ak}(X_j^{+i})]d\nu ,$$

where J_ν is the mean radiation intensity and $N(X_j^{+i})$ the number density of the species considered. The sum is taken over all k possible direct and Auger ionization routes, where $a_{\nu k}$ is the corresponding photoionization cross section as a function of frequency, $\nu_{0k}(X_j^{+i})$ the corresponding threshold frequency, and $h\nu_{Ak}(X_j^{+i})$ the energy of the released Auger electron when applicable (zero otherwise). To simplify notation, $a_{\nu k}(X_j^{+i})$ is assumed to be zero when ν is smaller than the threshold frequency $\nu_{0k}(X_j^{+i})$.

The total heating rate derived using these formulae corresponds, however, to an overestimate in the case of hard UV or X-ray photons because an ejected photoelectron (and the Auger electron when applicable) is likely to cause many secondary ionizations and line excitations before transferring its remaining energy to the electron gas, especially when the fraction of neutral hydrogen is relatively high ($\gtrsim 0.01$). Using the work of Shull (1979), who employed a Monte Carlo method to calculate the heating, secondary ionization, and Lyα excitation generated by the energetic electrons released with X-ray photoionization of interstellar gas, we introduced an efficiency factor in the computations that relates the fraction of energy actually deposited as heat into the gas, E_h, to the initial energy E of the photoelectron:

$$\epsilon(E, x) = \frac{E_h}{E} = \frac{\alpha_1(x)}{E} + \beta_1(x) ,$$

where x is the fractional ionization of hydrogen and α_1 and β_1 the coefficients given in Shull (1979). However, because the linear function given by Shull is not a good fit to the curves shown in his paper for $E < 100$ eV, the following formula was used instead:

$$\epsilon(E, x) = \beta_1(x) + \left[\frac{g(E)}{\alpha_1(x)} + \frac{1}{1 - \beta_1(x)}\right]^{-1} ,$$

where $g(E) = \text{Max}\,(0,\ E - \frac{3}{4}\ \text{ryd})$.

Since a fine binning of the UV spectrum was used, the integration in frequency was found to be very time-consuming, and to avoid having to repeat it when the fraction x or the ionic abundances $N(X_j^{+i})$ changed (or had to be found), a heating rate per ion of each ionic species was computed at the following x-values: 1.0, 0.1, 1×10^{-2}, 1×10^{-3}, and 1×10^{-4}:

$$\frac{G(x, X_j^{+i})}{N(X_j^{+i})} = \sum_{l=1}^{M} \int_{\nu_{1l}}^{\nu_{2l}} \frac{4\pi J_{\nu l}}{h\nu} \sum_k a_{\nu k}(X_j^{+i})\{\epsilon(h\nu_{Ak}(X_j^{+i}), x)h\nu_{Ak}(X_j^{+i}) + \epsilon(h\nu_{cl} - h\nu_{0k}(X_j^{+i}), x)[h\nu - h\nu_{0k}(X_j^{+i})]\}d\nu ,$$

where the summation in l is over the M energy bins, $J_{\nu l}$ is the mean intensity of radiation as a function of frequency within energy bin l (see § IV of this appendix), ν_{1l} and ν_{2l} are the lower and upper boundaries of bin l, and $h\nu_{cl}$ is the average energy of bin l. The efficiency factor ϵ for the photoelectron is evaluated using only average energy values for each bin, but this does not introduce any appreciable error in practice because of the small size of the bins. Note that, in the case of multiple production of Auger electrons from a single ionization route, only the Auger electron with the highest energy is included as $h\nu_{Ak}(X_j^{+i})$, the values of which can be found in Shull (1979).

To solve for the total heating rate G_T, it suffices to sum up the partial rates $G(x, X_j^{+i})$ using the abundances of the ionic species $N(X_j^{+i})$ when they are known and to interpolate the results (at the five x-values) using the actual x-value.

II. DETERMINATION OF THE RECOMBINATION AND IONIZATION RATES

The radiative and dielectronic recombination rates for He^0 and the metals are taken from the formulation of Aldrovandi and Péquignot (1973, 1976). For hydrogen and He^+, values given by Seaton (1959, 1962) are used.

Collisional ionization rates are obtained from the formulae of Cantó and Daltabuit (1974) and Franco and Daltabuit (1978), which have the virtue of simplicity and correct high-temperature behavior.

Twenty-four charge transfer reactions with H or He, taken mainly from the compilation of Butler and Dalgarno (1980) and Butler, Heil, and Dalgarno (1980), have been included. The temperature dependence of these rates is taken into account.

Photoionization rates are calculated using the parametric fit to the photoionization cross sections suggested by Seaton (1958). Parameters for photoionization from the valence shell are from Raymond (1976) and Osterbrock (1974). For inner-shell photoionization they are derived from the work of Weisheit (1974) and Daltabuit and Cox (1972).

The secondary ionization rate of hydrogen resulting from thermalization of energetic photoelectrons is derived from the work of Shull (1979), wherein the number ϕ_H of secondary ionizations of hydrogen atoms per primary photoelectron of energy E is given by the expression

$$\phi_H(E) = \text{Max}\,[0, (E/\text{ryd} - 1)\gamma(x)]\ ;$$

$\gamma(x)$ is an improved parametric fit to the curves $\phi_H(x)$ supplied by Shull (1979):

$$\gamma(x) = 0.478(1 - x^{-0.1\log_{10}(x)})\ ;$$

and x is the fractional ionization of hydrogen. Since ϕ_H is linear in E, the integration of ϕ_H/γ over the production rate of photoelectrons able to ionize hydrogen can be performed independently of x. For small changes with time in x, the secondary ionization rate r_H per neutral atom of hydrogen, then, is simply

$$r_H = \frac{\gamma(x)}{N_H(1-x)} S_H\ ,$$

with

$$S_H = \sum_{j,i} N(X_j^{+i}) P_H(X_j^{+i})\ ,$$

where $N(X_j^{+i})$ is the number density for the ionic species X_j^{+i} and $P_H(X_j^{+i})$ is the production rate per ion of photoelectrons able to ionize H times the number of possible ionizations per photoelectron; it is computed by the following integration:

$$P_H(X_j^{+i}) = \sum_{l=1} \int_{\nu_{1l}}^{\nu_{2l}} \frac{4\pi J_{\nu l}}{h\nu} \sum_k a_{\nu k}(X_j^{+i}) \left\{ \text{Max}\left[0, \frac{h\nu_{Ak}(X_j^{+i})}{\text{ryd}} - 1\right] + \text{Max}\left[0, \frac{h\nu_{cl} - h\nu_{0k}(X_j^{+i})}{\text{ryd}} - 1\right] \right\} d\nu\ ,$$

where the summation is carried over the M energy bins, $J_{\nu l}$ is the mean intensity of radiation as a function of frequency within the energy bin l (cf. § IV of this appendix), ν_{1l} and ν_{2l} are the lower and upper boundaries of bin l, $h\nu_{cl}$ is the average energy of bin l, $a_{\nu k}(X_j^{+i})$ is the kth photoionization cross section of ionic species X_j^{+i} as a function of frequency, $\nu_{0k}(X_j^{+i})$ is the corresponding threshold frequency, and $h\nu_{Ak}(X_j^{+i})$ is the energy of the released Auger electron (when applicable).

Even though the secondary ionization rates for heavier elements are not available in Shull's (1979) analysis, they can be estimated, at least for the lowest stages of ionization, in a way similar to that of Bergeron and Souffrin (1971) by using the ratio of the cross section for electroionization, $\sigma_{Y_j^{+i}}$, relative to that of hydrogen, σ_H; the ratio is evaluated at the average photoelectron energy $\langle E \rangle$:

$$r_{Y_j^{+i}} \approx r_H \frac{\sigma_{Y_j^{+i}}(\langle E \rangle)}{\sigma_H(\langle E \rangle)} \frac{S_{Y_j^{+i}}}{S_H}\ ,$$

where $S_{Y_j^{+i}}$ has a definition similar to that of S_H, except that the ionization potential of ion Y_j^{+i} is used wherever "ryd" appears in the definition of $P_H(X_j^{+i})$. To simplify the procedure, however, $S_{Y_j^{+i}}$ was derived instead from interpolation of the two quantities S_H and $S_{2.2\,\text{ryd}}$.

The integrations related to the secondary ionization rates, as well as those necessary to derive the photoionization and photoheating rates per ion (cf. § I of this appendix), which involve the radiation field, have been made independent of x in order to save computation time. Therefore, these time-consuming integrations need to be reevaluated only when the ionizing spectrum ($J_{\nu l}$) varies. For example, this makes it possible, when one starts from a nonequilibrium ionization structure, to follow easily in time the evolution of the ionic populations by allowing a quick recalculation at each time interval of all the rates, temperature and density, provided that the $J_{\nu l}$ are constant throughout the time intervals.

III. SOLUTION OF THE TIME-DEPENDENT IONIZATION BALANCE

Except for H and He, six ionization stages were considered for each of the following atomic elements: C, N, O, Ne, Mg, Si, S, Cl, and Ar. In most applications, however, the elements that have an ionization potential lower than hydrogen are not allowed to recombine to the neutral state.

Assuming that the total densities of the atomic elements and also the electron density remain constant in time, the ionization equation for each heavy element can be written in the differential form

$$\frac{d\boldsymbol{n}}{dt} = \mathbf{R}\boldsymbol{n}\ ,$$

where $\boldsymbol{n}$ is the column vector containing the ionic abundances (in this case, six were used) of the atomic element considered and $\mathbf{R}$ is the matrix containing the rates per ion (s^{-1}) corresponding to the changes in ionization stage allowed for the atomic element under consideration. Processes involving multiple ionization are easily taken into account in this formulation.

If we assume that the rates remain constant during some time step t (which implies no change of physical conditions or of abundances of the species with which charge transfer reactions take place), then the ionic abundances at the end of the time step, $\boldsymbol{n}_j$, are given in terms of the abundances at the start of the time step, $\boldsymbol{n}_i$, by (Pullman 1976)

$$\boldsymbol{n}_j = [\exp{(\mathbf{R}t)}]\boldsymbol{n}_i = \left[\mathbf{I} + \mathbf{R}t + \frac{(\mathbf{R}t)^2}{2!} + \frac{(\mathbf{R}t)^3}{3!} + \ldots\right]\boldsymbol{n}_i .$$

For large t, this series is not convergent. However, this can be resolved by expressing the solution in the following manner:

$$\boldsymbol{n}_j = \mathbf{T}^m\boldsymbol{n}_i = (\exp{\mathbf{O}})^m\boldsymbol{n}_i$$

where $\mathbf{O} = \mathbf{R}\delta$ and $m = t/\delta$, an integer ≥ 1. If δ is chosen such that none of the elements in the matrix $\mathbf{O}$ is greater than unity, convergence is assured. The expansion of the new series, for exp $\mathbf{O}$, is terminated at the level set by numerical precision in the computer. However, to raise the matrix $\mathbf{T}$ to the mth power would be a very time-consuming process, involving many matrix multiplications. It is advantageous to use a unit operator $\mathbf{U}$ such that

$$\mathbf{U}^l = \mathbf{T}^{kl} = \mathbf{T}^m$$

with k, l, m integers and $k \ll l$, giving

$$\boldsymbol{n}_j = \underbrace{\mathbf{UUU}\ldots\mathbf{U}}_{l\text{ times}}\boldsymbol{n}_i ,$$

where the multiplications are performed from right to left, involving the much faster multiplication of a matrix and a column vector.

This procedure is satisfactory and stable for time steps as long as $10^{15}/r_{\max}$ (with double precision on VAX 780), where $r_{\max}$ is the fastest rate in the matrix $\mathbf{R}$. To all practical purposes, such a time step defines ionization equilibrium when required, but with a much higher dynamic range in the relative sizes of the various ionic abundances than the methods commonly employed. [The latter often make use of terms of the type $(1 - f_k)$ for which the evaluation is limited by numerical precision in the computer.]

The ionization balance of hydrogen was treated in a different way. Since the electron density (given normal cosmic abundances) depends directly on the fractional ionization x of hydrogen, all rates depending on this density could not be assumed constant when x varied in time. The ionization equation in differential form is

$$\frac{dN_{\mathrm{H}^+}}{dt} = -\alpha_{\mathrm{H}} N_{\mathrm{H}^+} N_e + \theta_{\mathrm{H}} N_e N_{\mathrm{H}^0} + p_{\mathrm{H}} N_{\mathrm{H}^0} + r_{\mathrm{H}} N_{\mathrm{H}^0} + k_{\mathrm{H}} N_{\mathrm{H}^+} N_{\mathrm{H}^0} + \eta_{\mathrm{H}} N_e ,$$

where α_{H} is the recombination coefficient, θ_{H} the collisional ionization coefficient, p_{H} the photoionization rate per atom, r_{H} the secondary ionization rate per atom due to energetic photoelectrons, k_{H} the modified coefficient rate for charge transfer reactions (see below), and η_{H} the ionization rate correction per recombining electron (η_{H} is introduced only when the on-the-spot approximation is assumed and corresponds to the ionization resulting from the recombination and excitation photons of He I or He II; furthermore, α_{H} then takes the value of the recombination coefficient to excited states of hydrogen, α_B [Osterbrock 1974]). The electron density is defined as

$$N_e = N_{\mathrm{H}}(x + \delta) ; \qquad x = N_{\mathrm{H}^+}/N_{\mathrm{H}} , \qquad N_{\mathrm{H}} = N_{\mathrm{H}^+} + N_{\mathrm{H}^0} ,$$

where N_{H} is the total number density of hydrogen and δ is the component of the electron density that results from ionization of heavier elements. Assuming that the coefficients α_{H}, θ_{H}, p_{H}, r_{H}, k_{H}, η_{H}, and δ remain constant during a given time step, the ionization equation above is easily reduced to the form

$$\frac{dx}{dt} = A + Bx + Cx^2 .$$

A similar equation applies to the fraction of neutral hydrogen y, which must be solved for separately because its value is often too small to be simply derived from the expression $y = 1 - x$ (as a result of numerical precision in the computer). It is an important quantity, since the heating rate often depends on its value, however small it may be. In practice, four analytical solutions to the above differential equation had to be considered, depending on the values taken by the three coefficients A, B, and C.

When the time step is longer than is suitable for accurately following the evolution of the ionization balance of either hydrogen or the heavier elements, it is subdivided into subintervals and the ionization balance evolved successively for hydrogen and the other elements at each subinterval, in order to allow as close a coupling as possible between the two solutions; the charge transfer rates and all the rates depending on the electron density are recalculated at each subinterval.

The coupling resulting from charge transfer reactions represents a special problem, however. The solution proposed in Binette (1982) is very time-consuming. Instead, it is more appropriate to set the modified rate k_{H} above to zero, since these reactions can be shown to have little influence on the hydrogen balance.

The technique described here for the determination of the ionization balance of hydrogen and heavier elements is quite general and can be applied even to problems that presuppose ionization equilibrium. (It is, however, preferable to use a simpler solution when this is the case, since much computing time can be saved that way.) Multiple ionization is easily implemented. The solution to

the differential equations is mathematically exact (for each atomic element separately), while the other method commonly used (e.g., Cox 1972) deals with second-order integrated equations. In any event, the physical assumption of constant temperature and density within a given time step is not strictly valid for a cooling plasma but is of little consequence provided that the span in temperature is subdivided into a sufficient number of steps (where $\Delta T \ll T$) and that proper averages for the density, temperature, photon field, and net cooling rate are used within each time step. (The solution is iterated in order to check the convergence of these quantities when necessary.) Keeping the above quantities constant corresponds physically to allowing the gas to undergo partial relaxation at constant temperature during each time interval.

IV. RADIATION TRANSFER

The UV ionizing spectrum is divided into narrow energy bins that carry both the intensity of the UV ionizing source and the amount of radiation generated in the plasma itself.

The transfer of the ionizing ultraviolet and soft X-ray radiation is computed in 230 contiguous energy bins covering the range from 7.6 to 5000 eV. Each bin l contains the mean intensity J_l (ergs cm^{-2} sr^{-1} Hz^{-1} s^{-1}) evaluated at the center frequency of the bin, v_{cl}. Edges of the bins coincide with all the photoionization thresholds of the 11 atomic elements Additional bins were placed just above the ionization thresholds of H, He, C, N, O, Ne, and S, and where strong UV lines are expected. When integrating the ionizing spectrum in order to derive photoionization and photoheating rates, the mean intensity is represented as a power law inside each bin:

$$J(v) = J_l\left(\frac{v}{v_{cl}}\right)^{K_l} \qquad \text{for} \quad v_{1l} \leq v < v_{2l} ;$$

v_{1l} and v_{2l} are the lower and upper boundaries of bin l, and $v_{cl} = (v_{1l} + v_{2l})/2$. K_l is determined by using either the value J_{l-1} or J_{l+1}. [For all bins $(v_{2l} - v_{1l})/v_{cl} < 0.1$.]

As the ionizing flux becomes significantly absorbed far from the UV source, ionizing edges will start appearing in the UV spectrum corresponding to the different photoionization thresholds of the important absorbers. By the use of the simple method suggested here, the effect of these discontinuities is properly taken into account during integration, since only the value J_{l-1} or J_{l+1} that is on the same side of the discontinuity as J_l is used to determine K_l. Similar discontinuities also exist in the UV spectrum of the source itself when the latter corresponds to stellar atmosphere models (Hummer and Mihalas 1970), for example, or to a soft X-ray spectrum originating from an optically thin hot plasma (Raymond and Smith 1977). The ionizing flux resulting from line emission due to resonance or intercombination UV lines can become significant, and their presence easily detected in the UV spectrum, since the discontinuity exists for both J_{l-1} and J_{l+1}; K_l is then set to zero.

Since both the mean intensity J_ν and all the photoionization rates have power-law dependence on frequency, the integrations required to derive the photoionization or photoheating rates are carried out analytically within each energy bin; the total rates are obtained simply by summing up all the contributions from the different energy bins.

The mean intensity of the ionizing flux at any point in the ionized gas is made up of two components, the direct ionization by a UV source, on the one hand, and the integrated diffuse radiation field, on the other.

For the direct component the mean intensity J_{*l} for the energy bin l is given by

$$J_{*l}(r) = w(r) I_l(R_*) \exp(-\tau_l) ,$$

where τ_l is the integrated optical depth and w the geometrical dilution factor:

$$w(r) = \frac{1}{4}\left(\frac{R_*^2}{r^2}\right) \qquad \text{for } r \gg R_*$$

$$= \frac{1}{2}\left[1 - \left(1 - \frac{R_*^2}{r^2}\right)^{1/2}\right] \qquad \text{otherwise} ,$$

where R_* is the source radius and r ($r \geq R_*$) the distance between the position considered and the center of the ionizing source. $I_l(R_*)$ corresponds to the specific intensity (assumed here to be isotropic) at the center frequency v_{cl} of the energy bin l and evaluated at the surface of the source. If only the total luminosity of the source, L_l, is known, then one chooses R_* and r_0 (which is the radius at which the integration of the model starts), so that

$$I_l(R_*) = \frac{L_l}{(2\pi R_*)^2} \qquad \text{and} \qquad R_* \ll r_0 ;$$

when plane-parallel geometry is adopted for a model, w is set to $\frac{1}{2}$ (and $r_0 = 0$).

In the expression for $J_{*l}(r)$, τ_l corresponds to the integrated optical depth between r_0 and the position r (it is assumed that *no* absorbing matter exists between R_* and r_0):

$$\tau_l = \int_{r_0}^{r} \sum_{i,j} \sum_{k} a_{lk}(X_j^{+i}) N(X_j^{+i}) \epsilon \, dr ,$$

where ϵ is the volume filling factor ($\epsilon = \langle N \rangle^2 / \langle N^2 \rangle$) and a_{lk} is the kth photoionization cross section of atomic species X_j^{+i} evaluated at v_{cl}. The summation includes the heavy elements as well, since they become important absorbers at X-ray energies.

Several radiation processes contribute to the ionizing diffuse radiation field component within the cooling zone.

Photons generated by recapture of electrons were taken into account if the energy of the photon generated by recombination to the ground state exceeded 7.6 eV. In the case of helium, the contribution from recapture to level $n = 2$ of He II was also included ($h\nu = 3$ ryd). The Milne relation of detailed balance involving the photoionization cross section was used to derive the emission coefficients (Osterbrock 1974).

The ionizing continuum processes included are free-free and two-photon. For the former, we used the emission coefficient from Spitzer (1978) with a free-free Gaunt factor of unity (Karzas and Latter 1961). The two-photon processes which contribute to ionization are $2\,^2S$ of H I and He II, and $2\,^1S$ of He I.

The ionizing line processes we have included are all the collisionally excited (intercombination and resonance) lines with photon energies greater than 7.6 eV and the lines of He II Lyα (304 Å), He I λ584, and He I λ591 that result from recombination.

To simplify calculations, the spatial integration of the local emission is performed in a similar fashion to that of Tarter and Salpeter (1969), where half the emitted photons are artificially directed outward (downstream for a shock model) and the other half in the opposite direction (upstream), any angular dependence being neglected. Since the integration starts at the shock front and is carried through in the downstream direction, only the component that is emitted downstream (outward) can be calculated at any given point. Iteration of the entire model is required in a fully self-consistent model (Shull and McKee 1979) in order to provide the information needed to determine the upstream (inward) component. This is hardly necessary, however, since, by neglecting this component, one introduces an error typically of only a few percent in the line intensities of the Balmer lines as reported by Raymond (1976).

The diffuse downstream component is integrated step by step and accumulated into arrays. Within a given space step, however, where average values of temperature, density, and radiation field are needed to calculate the ionization balance, one can assume that the local upstream component generated is equal in intensity to the downstream one, and calculate an appropriate average diffuse radiation field valid for the space step considered by adding together the two components emitted locally.

Once an average ionization balance, temperature, and densities that converge within a space step are derived, the diffuse downstream radiation field is integrated using the formula given by radiation transfer through a uniform slab and the absorption coefficient σ_l (cm^{-1}) defined as follows:

$$\sigma_l = \frac{d\tau_l}{dr} = \sum_{i,j} \sum_{k} a_{lk}(\mathrm{X}_j^{+i}) N(\mathrm{X}_j^{+i}) \, .$$

At each step of a given model, the contribution of the locally emitted UV radiation is also added to the intensity of the upstream component $I_{\mathrm{UP}}(r_0)$ (as seen from the shock front at r_0), in order to derive self-consistent preionization values if global iterations of the models are envisaged.

The ultraviolet resonance lines are the object of a separate solution to the radiation transfer equation, and their intensities are kept in distinct energy bins. The main effect of the resonance scattering on line photons is to decrease their penetrating power. This is taken into account by assuming that the mean travel length of a resonant photon across a slab is of the order of $Q\delta r$, where Q is the mean number of scatterings experienced inside the slab. Consequently, the probability of absorption is increased by the same factor Q, and the absorption coefficient, used in the equations above for the solution of the radiation transfer for resonance lines, becomes

$$\sigma_l' = Q\sigma_l \, ,$$

with $Q \approx 1/E$, where E is the mean escape probability through a uniform slab and is given in Capriotti (1965) as a function of optical path length τ_0 for scattering. The function can be approximated by

$$E = 1.0 + 0.71\tau_0 \ln(2\tau_0) + [\![\{[(0.00048\tau_0 - 0.019876)\tau_0 + 0.08333]\tau_0 - 0.3849\}\tau_0 - 0.83]\!]\tau_0 \qquad (\tau_0 < 1.5) \, ,$$

$$= \{0.14 + 0.25/[\ln(2\tau_0)] + [\ln(2\tau_0)]^{1/2}\}/(3.5449\tau_0) \qquad (\tau_0 \geq 1.5)$$

(Capriotti 1965; Netzer 1975); τ_0 is defined as follows:

$$\tau_0 = N_a b_{\nu_0} \epsilon \delta r \, ,$$

with

$$b_\nu = \frac{\pi^{1/2} e^2 f_a}{m_e \nu_0 \nu_{\mathrm{D}}} \left[1 - \exp\left(\frac{h\nu_0}{kT}\right)\right]$$

$$= 3.0 \times 10^{-18} \frac{f_a}{\nu_{\mathrm{D}} h\nu_0} \left[1 - \exp\left(\frac{h\nu_0}{kT}\right)\right] ,$$

$$\nu_{\mathrm{D}} = \frac{2kT}{m_a} \, .$$

(We note that a simple Doppler broadening function is adopted for the scattered photons.) In the above equations m_a is the mass of the absorbing atom, T is the temperature, N_a is the number density of absorbers, and f_a is the absorption oscillator strength for the resonance line under consideration. It must be emphasized however, that in the more general situation of a medium in expansion or contraction, a reduced optical path length τ_0' ought to be determined instead, because a uniform velocity gradient has the effect of continuously shifting out the frequency of the average line photon relative to the absorbers' rest frame, thus increasing the mean

escape probability. Making use of Capriotti's (1965) analysis of the problem of expanding shells, we can write

$$\tau_x = \tau_0(v_D/\delta v)\int_{x-\delta v/v_D}^{x} \exp(-y^2)dy ;$$

setting $x = v_0$, we obtain

$$\tau_0' \approx \tau_0 \frac{\pi^{1/2}}{2}\left[\frac{\mathrm{erf}(\delta v/v_D)}{\delta v/v_D}\right],$$

with $\delta v \approx \delta r(\partial v/\partial r)_r$, where δv is the variation in the velocity of the medium across a slab of thickness δr. For example, with $\delta v/v_D = 3$, one gets $\tau_0' \approx 0.5\tau_0$, which implies an increased mean escape probability for the average line photon.

REFERENCES

Aldrovandi, S. M. V., and Péquignot, D. 1973, *Astr. Ap.*, **25**, 137.
———. 1976, *Astr. Ap.*, **47**, 321.
Allen, C. W. 1973, *Astrophysical Quantities* (3d ed.; London: University of London Press).
Baker, J. G., and Menzel, D. H. 1938, *Ap. J.*, **88**, 52.
Baldwin, J. A., Phillips, M. M., and Terlevich, R. 1981, *Pub. A.S.P.*, **93**, 5.
Bergeron, J., and Souffrin, S. 1971, *Astr. Ap.*, **14**, 167.
Bhatia, A. K., Doschek, G. A., and Feldman, U. 1979, *Astr. Ap.*, **76**, 359.
Binette, L. 1982, Ph.D. thesis, Australian National University, Canberra.
———. 1984, *The Messenger*, **38**, 13.
———. 1985, *Astr. Ap.*, **143**, 334.
Binette, L., Dopita, M. A., D'Odorico, S., and Benvenuti, P. 1982, *Astr. Ap.*, **115**, 315.
Blanco, V. M., Graham, J. A., Laskar, B. M., and Osmer, P. S. 1975, *Ap. J. (Letters)*, **198**, L63.
Brocklehurst, M. 1971, *M.N.R.A.S.*, **153**, 471.
Butler, S. E., and Dalgarno, A. 1980, *Ap. J.*, **241**, 838.
Butler, S. E., Heil, T. G., and Dalgarno, A. 1980, *Ap. J.*, **241**, 442.
Butler, S. E., and Raymond, J. C. 1980, *Ap. J.*, **240**, 680.
Canizares, C. R., Clark, G. W., Jernigan, J. G., and Markert, T. H. 1982, *Ap. J.*, **262**, 33.
Cantó, J., and Daltabuit, E. 1974, *Rev. Mexicana Astr. Ap.*, **1**, 5.
Capriotti, E. R. 1965, *Ap. J.*, **142**, 1101.
Chevalier, R. A., and Theys, J. C. 1975, *Ap. J.*, **195**, 53.
Contini, M., and Aldrovandi, S. M. V. 1983, *Astr. Ap.*, **127**, 15.
Cox, D. P. 1972, *Ap. J.*, **178**, 143.
Daltabuit, E., and Cox, D. P. 1972, *Ap. J.*, **177**, 855.
Daltabuit, E., MacAlpine, G. M., and Cox, D. P. 1978, *Ap. J.*, **219**, 372.
Demoulin-Ulrich, M.-H., Butcher, H. R. and Boksenberg, A. 1984, *Ap. J.*, **285**, 527.
Dopita, M. A. 1976, *Ap. J.*, **209**, 395.
———. 1977, *Ap. J. Suppl.*, **33**, 437.
Dopita, M. A., Binette, L., D'Odorico, S., and Benvenuti, P. 1984, *Ap. J.*, **276**, 653.
Dopita, M. A., Binette, L., and Schwartz, R. D. 1982, *Ap. J.*, **261**, 183.
Dopita, M. A., Binette, L., and Tuohy, I. R. 1984, *Ap. J.*, **282**, 142.
Dopita, M. A., Mason, D. J., and Robb, W. D. 1976, *Ap. J.*, **207**, 102.
Draine, B. T. 1981, *Ap. J.*, **245**, 880.
Eissner, W., and Seaton, M. J. 1974, *J. Phys. B.*, **7**, 2533.
Fabian, A. C., and Nulsen, P. E. J. 1977, *M.N.R.A.S.*, **180**, 479.
Field, G. B. 1965, *Ap. J.*, **142**, 531.
Ford, H. C., and Butcher, H. 1979, *Ap. J. Suppl.*, **41**, 147.
Franco, J., and Daltabuit, E. 1978, *Rev. Mexicana Astr. Ap.*, **2**, 325.
Graham, J. A., and Price, R. M. 1981, *Ap. J.*, **247**, 813.
Gronenschild, E. H. B. M. 1979, *Astr. Ap.*, **77**, 53.
Gronenschild, E. H. B. M., and Mewe, R. 1982, *Astr. Ap. Suppl.*, **48**, 305.
Hamilton, A. J. S., Sarazin, C. L., and Chevalier, R. A. 1983, *Ap. J. Suppl.*, **51**, 115.
Heckman, T. M. 1980, *Astr. Ap.*, **87**, 152.
Hummer, D. G., and Mihalas, D. M. 1970, *M.N.R.A.S.*, **147**, 339.
Itoh, H. 1979, *Pub. Astr. Soc. Japan*, **31**, 541.
Johnson, L. C. 1972, *Ap. J.*, **174**, 2237.
Karzas, W. J., and Latter, R. 1961, *Ap. J. Suppl.*, **6**, 167.
Keel, W. C. 1983*a*, *Ap. J.*, **268**, 632.
———. 1983*b*, *Ap. J.*, **269**, 466.
Kent, S. M., and Sargent, W. L. W. 1979, *Ap. J.*, **230**, 667.
Kleinpoppen, H., and Kraiss, E. 1967, *Phys. Rev. Letters*, **20**, 361.
MacAlpine, G. M. 1972, *Ap. J.*, **175**, 11.
Mathews, W. G. 1978, *Ap. J.*, **219**, 413.
Mathews, W. G., and Bregman, J. N. 1978, *Ap. J.*, **224**, 308.
McCray, R., Stein, R. F., and Kafatos, M. 1975, *Ap. J.*, **196**, 565.
Mendoza, C. 1983, in *IAU Symposium 103, Planetary Nebulae*, ed. D. R. Flower (Dordrecht: Reidel), p. 143.
Mendoza, C., and Zeippen, C. J. 1982, *M.N.R.A.S.*, **198**, 127.
Mufson, S. L. 1975, *Ap. J.*, **202**, 372.
Netzer, H. 1975, *M.N.R.A.S.*, **171**, 395.
Nussbaumer, H., and Rusca, C. 1979, *Astr. Ap.*, **72**, 129.
Nussbaumer, H., and Storey, P. J. 1983, *Astr. Ap.*, **126**, 75.
Osmer, P. S. 1978, *Ap. J. (Letters)*, **226**, L79.
Osterbrock, D. E. 1974, *Astrophysics of Gaseous Nebulae* (San Francisco: Freeman).
Osterbrock, D. E., and Miller, J. S. 1975, *Ap. J.*, **197**, 535.
Péquignot, D. 1980, *Astr. Ap.*, **81**, 356.
Péquignot, D., Stasińska, G., and Aldrovandi, S. M. V. 1978, *Astr. Ap.*, **63**, 313.
Pradhan, A. K. 1976, *M.N.R.A.S.*, **177**, 31.
———. 1978, *M.N.R.A.S.*, **183**, 89P.
Pullman, N. J. 1976, *Matrix Theory and Its Applications: Selected Topics* (New York: Dekker).
Raymond, J. C. 1976, Ph.D. thesis, University of Wisconsin, Madison.
———. 1979, *Ap. J. Suppl.*, **39**, 1.
Raymond, J. C., Cox, D. P., and Smith, B. W. 1976, *Ap. J.*, **204**, 290.
Raymond, J. C., and Smith, B. W. 1977, *Ap. J. Suppl.*, **35**, 419.
Schwartz, J., McCray, R., and Stein, R. F. 1972, *Ap. J.*, **175**, 673.
Seaton, M. J. 1958, *Rev. Mod. Phys.*, **30**, 979.
———. 1959, *M.N.R.A.S.*, **119**, 81.
———. 1962, *M.N.R.A.S.*, **125**, 437.
———. 1975, *M.N.R.A.S.*, **179**, 475.
Shull, J. M. 1979, *Ap. J.*, **234**, 761.
———. 1980, *Ap. J.*, **237**, 769.
Shull, J. M., and McKee, C. F. 1979, *Ap. J.*, **227**, 131.
Smith, M. W., and Wiese, W. L. 1971, *Ap. J. Suppl.*, **23**, 103.
Spitzer, L. 1978, *Physical Processes in the Interstellar Medium* (New York: Wiley).
Stauffer, J. R. 1982, *Ap. J.*, **262**, 66.
Stewart, G. C., Fabian, A. C., Jones, C., and Forman, W. 1984, *Ap. J.*, **285**, 1.
Tarter, C. B. 1969, *Ap. J. Suppl.*, **18**, 1.
Tarter, B. C., and Salpeter, E. E. 1969, *Ap. J.*, **156**, 953.
Weisheit, J. C. 1974, *Ap. J.*, **190**, 735.
Wiese, W. L., Smith, M. W., and Glennon, B. M. 1966, *Atomic Transition Probabilities*, Vol. **1** (NSRDS–NBS 4).
Zeippen, C. J. 1982, *M.N.R.A.S.*, **198**, 111.

L. Binette: European Southern Observatory, Karl-Schwarzschild-Strasse 2, D8046 Garching bei München, Federal Republic of Germany

M. Dopita and Ian R. Tuohy: Mount Stromlo and Siding Spring Observatories, Private Bag, Woden P.O., ACT 2606, Australia